

## Supplementary material

### **A flexible two-photon fiberscope for fast activity imaging and precise optogenetic photostimulation of neurons in freely moving mice**

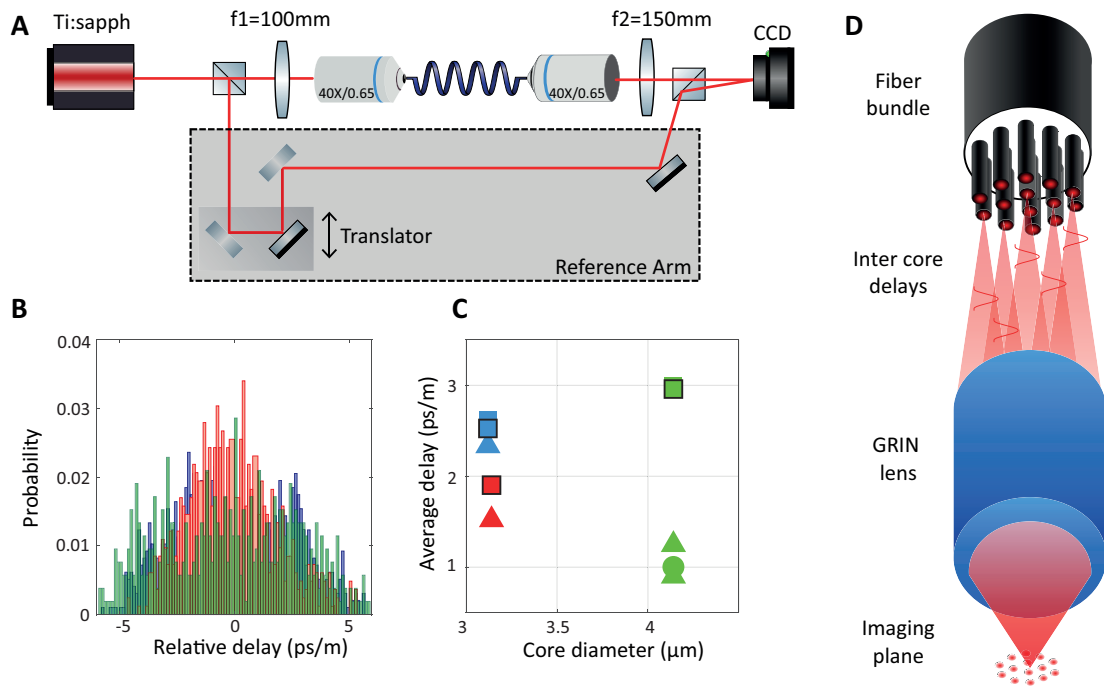
Nicolò Accanto<sup>1\*</sup>, François G. C. Blot<sup>1\*</sup>, Antonio Lorca-Cámara<sup>1\*</sup>, Valeria Zampini<sup>1</sup>, Florence Bui<sup>1</sup>, Christophe Tourain<sup>1</sup>, Noam Badt<sup>2</sup>, Ori Katz<sup>2</sup>, and Valentina Emiliani<sup>1</sup>

<sup>1</sup> Sorbonne Université, INSERM, CNRS, Institut de la Vision, F-75012 Paris, France

<sup>2</sup> Department of Applied Physics, Hebrew University of Jerusalem, Jerusalem 9190401, Israel.

\* These authors contributed equally

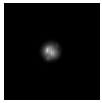
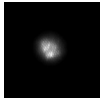
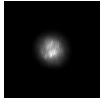
Contact: nicolo.accanto@inserm.fr, valentina.emiliani@inserm.fr

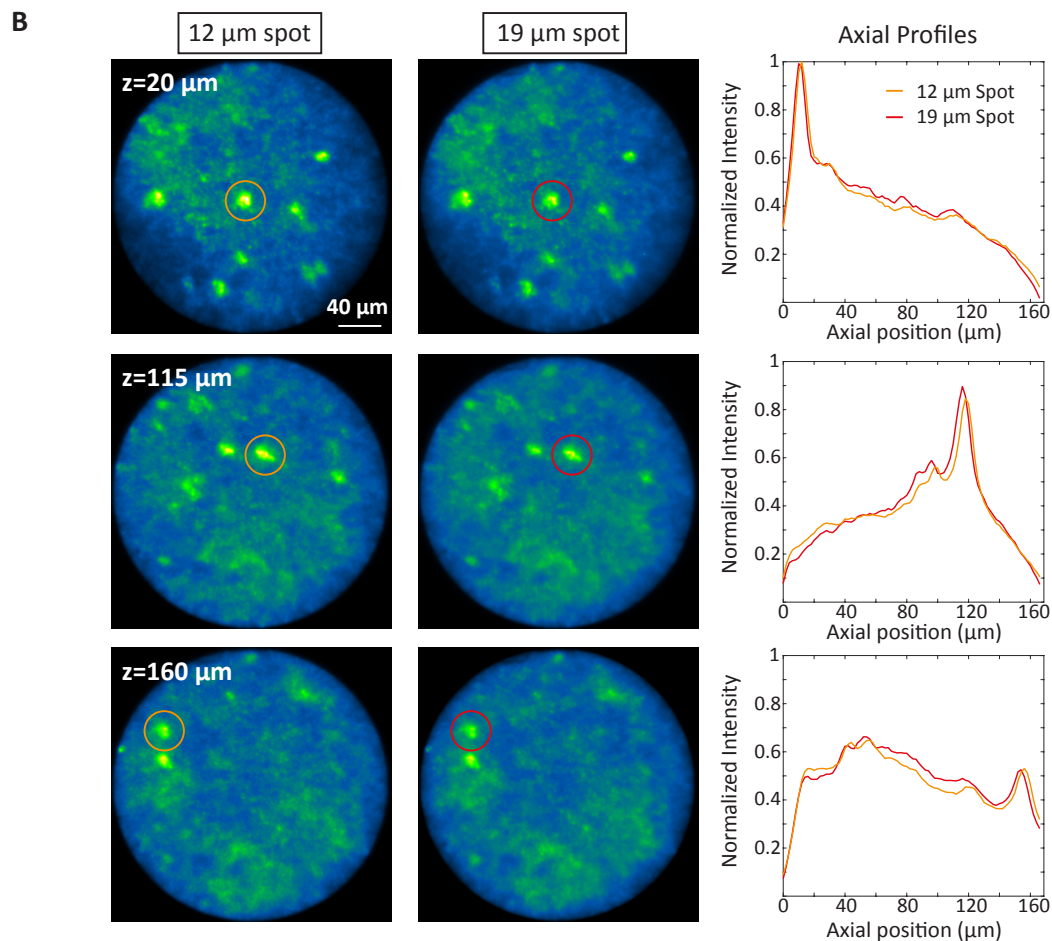


**Supplementary Figure 1** | *Characterization of inter core delay dispersion for different Fujikura fibers.*

**A.** Interferometric setup used for measuring the inter core delay dispersion. A Ti:sapph laser was split into two arms. One arm was sent through the fiber bundle, and the reference arm was delayed using an adjustable delay line. **B.** Distribution of the pulse arrival time in the first mode through the different cores measured for three different Fujikura fiber bundles models: green FIGH-10-500N; red: FIGH-06-300S; blue: FIGH-03-215S). **C.** Average pulse delay for each fiber bundle, defined as the standard deviation of the distribution in (B). The average pulse delay is given in picosecond per meter of fiber and plotted against the core diameter, which is specific of different fiber bundle models. Triangles, squares and circles mark fiber lengths of 0.3, 0.6, 1.82 m respectively. The symbols corresponding to fibers from figure (B) are surrounded by a black contour line. For all the measured bundles, the average pulse delay per meter of fiber is  $> 1$  ps, from which it is apparent that a 2 m long fiber bundle should decouple the cores in time of a sufficient amount to maintain good axial resolution for spatially extended 2P excitations, especially when using  $\sim 150$  fs laser pulses. **D.** Sketch of different fiber bundle cores, illuminated at the same time and re-imaged at the sample plane by using the GRIN lens in the 2P-FENDO configuration. The pulse from each core is coupled out at a slightly different time. The GRIN lens effectively acts as a doublet, making an image of the output facet of the fiber bundle onto the sample plane, with a certain demagnification factor (2.2 or 4.5 depending on the GRIN lens used). Because the beamlet from each core travels with a certain temporal delay, they do not interfere with each other on the way to the sample plane, thus avoiding out of focus excitation. Related to **Fig. 1**.

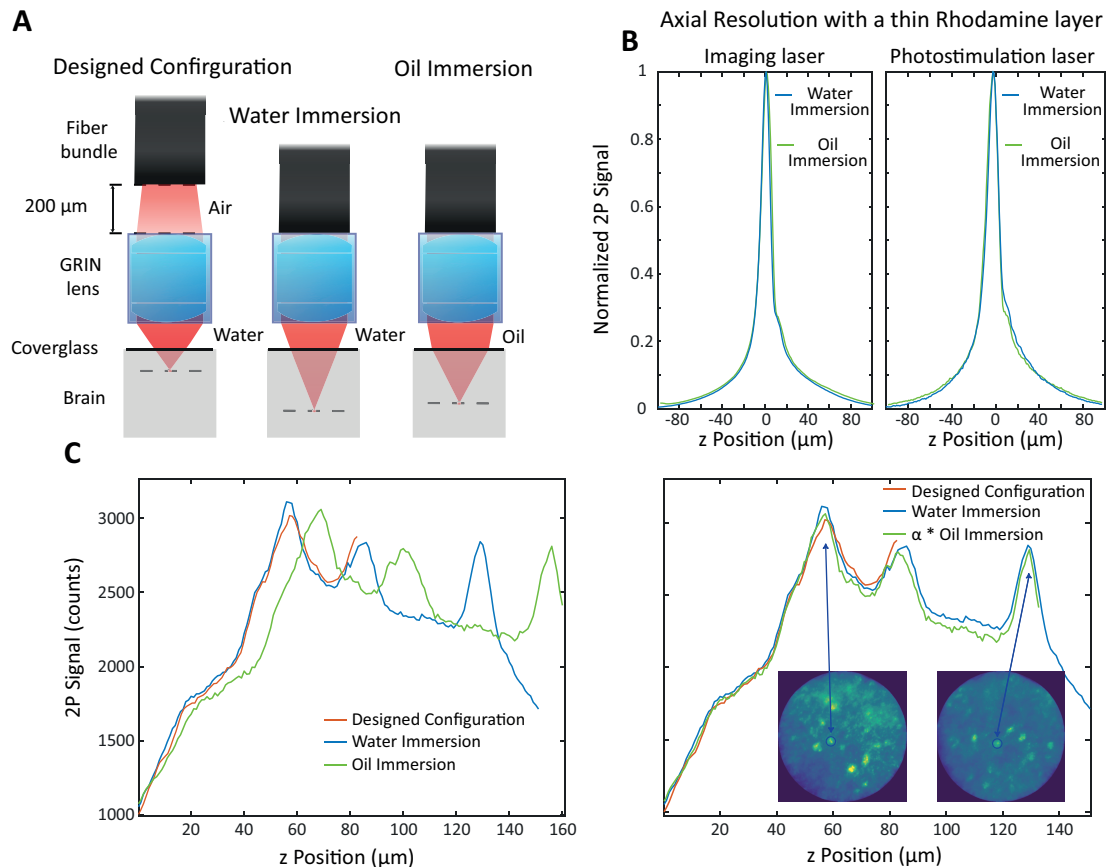
**A**

| Power before fiber | Power after fiber | Power scanning | Spot size at sample | N cores illuminated | Static spot   |
|--------------------|-------------------|----------------|---------------------|---------------------|---|
| 400 mW             | 140 mW            | 70 mW          | 12 $\mu\text{m}$    | 34                  |  |
| 700 mW             | 240 mW            | 120 mW         | 15 $\mu\text{m}$    | 54                  |  |
| 1000 mW            | 350 mW            | 170 mW         | 19 $\mu\text{m}$    | 86                  |  |



**Supplementary Figure 2** | *Characterization of 2P imaging for different spot sizes.*

**A.** Power measurements for the imaging laser for different spot sizes at the sample plane and at different points in the setup when using GRIN lens 2. The coupling objective, fiber bundle, and GRIN lens system transmit  $\sim 35\%$  of the light, and an additional factor of 2 is lost when scanning the imaging beam on a larger area than the fiber bundle (see **STAR Methods**). **B.** Three images of a  $z$ -stack of a GFP slice at different depths for a small and a large imaging spot. The same features are visible in the two conditions for the same plane, confirming that the axial confinement is comparable. On the right we plot the axial profiles for the cells circled in the images. For a small and a large imaging spots, the axial profiles largely overlap, excluding additional background when using larger imaging spots. Related to **Fig. 2**.



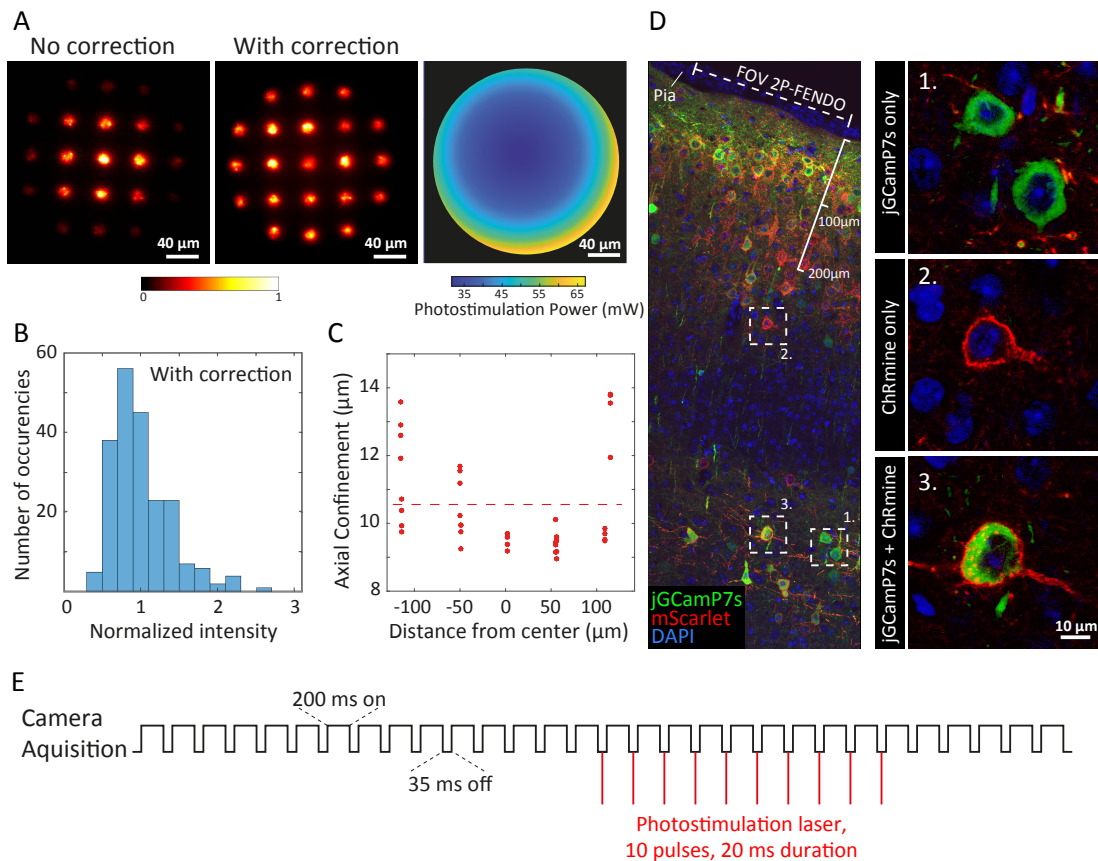
**Supplementary Figure 3** | *Fiber bundle and GRIN lens configurations.*

**A.** Scheme of the different configurations used in the experiments. The ‘designed configuration’ refers to the designed parameters according to the manufacturer: the fiber bundle is at the distance of 200  $\mu\text{m}$  from the GRIN lens and the tip of the GRIN lens is immersed in water. It is the configuration leading to the shallower working distance below the cover glass. In the ‘water immersion’ configuration the fiber is in contact with the GRIN lens and the tip of the GRIN lens is immersed in water. It is the configuration that results in the largest working distance below the cover glass. In the ‘oil immersion’ configuration, the fiber is in contact with the GRIN lens and the tip of the GRIN lens is immersed in oil. This is the configuration used for freely moving experiments to avoid water evaporation (see also **STAR Methods**). **B.** Axial resolution for imaging (*left*) and photostimulation laser (*right*) through GRIN lens 2 in either the oil (green) or the water (blue) immersion configuration, measured on a thin rhodamine layer, showing no difference in axial resolutions. **C.** Characterization of the effective working distance for the 3 different configurations illustrated in A, measured from z-stacks on  $\sim 150 \mu\text{m}$  thick GCaMP6 brain slices. The axial profiles in the left-hand plot show 3 different peaks corresponding to cells on different planes that are at the same  $xy$  locations. Three effects are apparent: 1) the designed configuration (red curve) has the shortest working distance, allowing to resolve only one peak until the depth of 80  $\mu\text{m}$  below the cover glass; 2) the water immersion configuration (blue curve) is the one producing the largest working distance, allowing to measure three different peaks and to resolve at least 20  $\mu\text{m}$  below the last peak (located at  $z = 130 \mu\text{m}$ ); 3) the oil immersion configuration (green curve) is able to resolve three peaks, but it can only measure few  $\mu\text{m}$  below the last peak, moreover the  $z$  axis in the oil immersion configuration is distorted with respect to the water immersion case. As explained in **STAR Methods**, due to the index mismatch between oil and brain tissue on the two

sides of the cover glass, a vertical displacement of the endoscope (fiber bundle + GRIN lens) of a quantity  $\Delta z$  with respect to the sample produces a focal shift of  $\alpha * \Delta z$  with  $\alpha < 1$ . In the right-hand plot, we multiplied the  $z$  axis for the oil immersion configuration by the factor  $\alpha = 0.83$ , to match the positions of the peaks measured with the water immersion configuration. The found value is consistent with the theory

of that predicts  $\alpha = \frac{\sqrt{n_b^2 - NA^2}}{\sqrt{n_o^2 - NA^2}} = 0.87$ , considering the refractive index of the brain

$n_b = 1.35$ , the refractive index of the oil  $n_o = 1.5$  and the numerical aperture of the GRIN lens  $NA = 0.7$ . The insets in the right-hand plots show two different planes in the  $z$ -stack, with the circled cells corresponding to the axial peaks indicated by the arrows. Related to **Fig. 3** and **4**.



**Supplementary Figure 4** | *Spatial resolution and temporal presentation of the holographic photostimulation.*

**A.** 2P excited fluorescence generated on a uniform thick fluorescent slide from a distribution of  $15 \mu\text{m}$  holographic spots without (*left*) and with (*middle*) intensity correction applied on the SLM. The SLM corrects both for the diffraction efficiency and the lower signal at the edges of the FOV (consequence of the larger aberration of the GRIN lens as one moves away from the center). *Right*: Effective power distribution used to photostimulate neurons, measured at the GRIN lens output. In the center of the FOV we used 30 or 40 mW (in the figure we give the case for 30 mW), which were increased smoothly away from the center to generate the same amount of 2P signal.

**B.** Distribution of the 2P excited fluorescence from different holographic spots generated with the SLM after the application of the intensity correction.

**C.** Axial resolution of holographic spots as a function of the distance from the center. The red dots correspond to individual measurements taken in different days. The dashed line is the average over all the different measurements.

**D.** Distribution of transduced cells in the wS1 cortex of mice injected with AAV9-syn-jGCaMP7s-WPRE and AAV1-hSyn-ChRmine-mScarlet-Kv2.1-WPRE. The diameter of 2P-FENDO field of view is delineated by the white dotted line. Depth from the brain surface below the pia is indicated to represent the cell distribution in the depth range of 2P-FENDO. Example cells illustrating jGCaMP7s expression only (1.), ChRmine expression only (2.) or jGCaMP7s + ChRmine (3.). Scale bar =  $10 \mu\text{m}$ .

**E.** Photostimulation protocol and camera acquisition timing. During photostimulation experiments, the EM-CCD camera was driven in external exposure mode, in which a TTL signal, similar to the black curve in figure, was supplied to the camera trigger input. The camera was forced

to expose for 200 ms and to remain off for 35 ms. A second signal, synchronized with the camera was then sent to a fast shutter that controlled the photostimulation laser transmission. The shutter was open for 10 times for 20 ms, in correspondence with camera off times, as shown by the red lines in figures. Related to **Fig. 6**

| Mouse N | Measurement days | Type of experiment | Imaging depth ( $\mu\text{m}$ ) | Imaging power at fiber exit (mW) | Data in figures               |
|---------|------------------|--------------------|---------------------------------|----------------------------------|-------------------------------|
| 1       | 2                | Imaging only       | 80 $\pm$ 10                     | 100-140                          | Fig. 4C, Video S2             |
| 2       | 5                | Imaging/Photostim  | 70 $\pm$ 10                     | 85-120                           | Fig. 4A, Fig.6A-E, VideoS2-S3 |
| 3       | 2                | Imaging/Photostim  | 125 $\pm$ 10                    | 110-155                          | Fig. 6C-E                     |
| 4       | 2                | Imaging/Photostim  | 70 $\pm$ 10                     | 85-100                           | Fig. 6C-E                     |

**Supplementary Table 1. Data used.** *Summary of the parameters used in all the measurements shown in the main manuscript.* Related to **Fig. 4, 5 and 6.**

**Supplementary Video 1.** *In vivo* stack acquisition with 2P-FENDO

*In vivo* stack acquisition of TdTomato expressing neurons in V1 taken with GRIN1 lens, or GFP expressing neurons with either GRIN 1 or GIRN 2 lenses. Depth of imaging is indicated in the upper left corner. The images were filtered with a gaussian blur function to get rid of the core structure of the fiber bundle and normalized for each plane. Related to **Fig. 3.**

**Supplementary Video 2.** Spontaneous activity recording at 2 Hz, 5 Hz, and 20 Hz with 2P-FENDO in a freely moving mouse.

The calcium data were motion corrected with CaImAn. We applied a 3-frame running average using the Image J plugin. Both the calcium imaging video and the video of the mouse moving in the cage were sped up  $\sim 8$  times. Related to **Fig. 4.**

**Supplementary Video 3.** High-resolution, multi-cell holographic photostimulation with 2P-FENDO, in a freely moving mouse. The calcium data were motion corrected with CaImAn. We applied a 3-frame running average using the Image J plugin. Both the calcium imaging video and the video of the mouse moving in the cage were sped up  $\sim 7$  times. The video corresponds to the calcium traces reported in Fig. 4 a of the main manuscript. In the calcium images, arrows appear few seconds before the photostimulation laser is switched on and point at the photostimulated cells. The traces in the lower panel correspond to the  $dF/F$  signal of the targeted (red traces) and untargeted (white traces) neurons. Related to **Fig. 6.**